Bioorganic & Medicinal Chemistry Letters 28 (2018) 1581–1590

Contents lists available at ScienceDirect

Bioorganic & Medicinal Chemistry Letters

journal homepage: www.elsevier.com/locate/bmcl

Structural analysis and antioxidant activity of the glycoside from *Imperial Chrysanthemum*

Zhen-Yuan Zhu [a,*], Li-Chao Pan [a], Yun-Tang [a], Yong-min Zhang [b]

[a] Key Laboratory of Food Nutrition and Safety, Ministry of Education, College of Food Science and Biotechnology, Tianjin University of Science and Technology, Tianjin 300457, PR China
[b] Université Pierre et Marie Curie-Paris 6, Institut Parisien de Chimie Moléculaire UMR CNRS 7201, 4 place Jussieu, 75005 Paris, France

ARTICLE INFO

Article history:
Received 25 October 2017
Revised 14 December 2017
Accepted 21 March 2018
Available online 22 March 2018

Keywords:
Imperial Chrysanthemum glucoside
Isolation and purification
Antioxidant
Molecular structure

ABSTRACT

A new glycoside, named as CG-1, was separated from *Imperial Chrysanthemum* with silica gel column chromatography. The purity was detected by TLC and HPLC. The crystal shape of CG-1 was consisting of a quadrangular and two rectangular pyramids. The analysis of DSC and TGA showed that the melting point of CG-1 crystal was 150.22 °C and had good thermal stability. The monosaccharide conformation analysis showed that it was D-glucose. The structure characteristics were compared by FT-IR, NMR spectroscopy and LC-MS and a molecular structure has been deduced which consistent with spectroscopic results. In vitro antioxidant results suggested that the glycoside extracted from *Imperial Chrysanthemum* could be effectively employed as natural antioxidant in health or functional food. This work is of significance to keep the antioxidant activity in the processing and application of *Imperial Chrysanthemum*.

© 2018 Elsevier Ltd. All rights reserved.

Introduction

Under normal circumstances, free radical production and scavenging is a dynamic equilibrium in vivo. Low concentration of free radicals not only does not damage the body, but also shows unique physiological functions.[1] Excessive production of free radicals can react with lipids, proteins and DNA, leading to several diseases, such as can induce many human diseases such as cardiovascular disease,[2] cancer,[3,4] respiratory inflammation,[5] and DNA damage.[6] Antioxidants can alleviate the oxidative stress, so the research and development of antioxidants was closely related to healthy living. However, some currently used synthetic free radical scavengers have been demonstrated various side effects.[7] Natural products derived from plants are generally considered to be less toxic and have fewer side effects than synthetic medicines.[8,9] Therefore, natural antioxidants were more acceptable in modern healthy lifestyle. Natural glycosides, such as flavonoid glycosides, iridoid glycosides, phenolic glycosides, quercetin glycosides and so on, showed good antioxidant activity.[10–13] *Imperial Chrysanthemum* is a traditional Chinese medicinal herb of the family *Compositae* with dried anthodium of Ramat. It contains several of natural active ingredients and has been used extensively in foods, tea and tea drinks. *Imperial Chrysanthemum*, as natural antioxidant food, shows the advantages which don't exist in other synthetic antioxidants.[14,15] Chrysanthemum glucoside, as a large class in numerous bioactive compounds in chrysanthemum, has a great effect on antioxidation.[16,17] In order to maintain and improve the antioxidant capacity, the processing technic and culture techniques of chrysanthemum were constantly perfected.[18–20] The extraction, isolation and purification of glycosides, having antioxidant effects in *Imperial Chrysanthemum*, are important to develop the resources and its effective components. The analysis of structure and determination of functional components of the *Imperial Chrysanthemum* glucoside by modern instrument analysis have great significance for the application and development of antioxidant capacity of *Imperial Chrysanthemum*. This article mainly studied and discussed the separation and purification of the main small molecular glycosides extracted from *Imperial Chrysanthemum*. And the molecular structures of the products were determined by IR, NMR, MS and HPLC. This article also conducts the preliminary research and the exploration about the antioxidant activity of the extracts.

Materials and methods

Imperial Chrysanthemum is produced in xuzhou, jiangsu province of China.

Chemistry

All chemicals (reagent grade) used were purchased from Sigma-Aldrich (U.S.A) and Aladdin-Reagent Co., Ltd (China). TLC (Thin

* Corresponding author.
E-mail address: zhyuanzhu@tust.edu.cn (Z.-Y. Zhu).

https://doi.org/10.1016/j.bmcl.2018.03.059
0960-894X/© 2018 Elsevier Ltd. All rights reserved.

layer chromatography) was run on the silica gel coated aluminum sheets (Silica Gel 60 GF, E, Merck, Germany). ^{1}H NMR and ^{13}C-NMR were recorded on a Bruker AVANCE instrument (400 MHz). ESI (Electrospray Ionization) mass spectra were obtained on an LCQ-Advantayc-MAX (LAM10188, Finnigan, Co., Ltd, USA).

Method

Separation by silica gel column chromatography

The pulverized *Imperial Chrysanthemum*, which proper granularity was in 200–300 mesh, was used as raw material. Objective to get the extract from *Imperial Chrysanthemum* with the conditions are as follows: taking 80% ethanol as a solvent, extraction time 180 min and the ratio of material to solution is 1:20. Repeat three times, merge all the extract and concentrate through the methods of reduced pressure concentration.

For TLC analysis, 10 × 20 cm TLC plate (GF) was cut into properly size. 2 μL of the samples were spotted in 1 cm above the bottom of the plate with a microliter syringe. After sample dried, vertically placed the TLC plate in a normal chromatographic chamber that was pre-saturated in the developing solvent, before the final solvent climbed to the position, which is 1 cm distant from the top of thin plate. Remove the thin plate into Chromogenic agent and take it out quickly for air-dry. The plate appeared color when heated with electromagnetic oven.[21–23] According to the separating effect and the value of R_f, making changes in developing agents and choosing a correct developing agent as the mobile phase of the silica gel column chromatography (SGCCT). Then adopt silica gel column chromatography and recrystallization for separation and purification of extract.

A glass column (40 cm × 3.0 cm) was packed with prepared dry packing silica gel (45 g, 200–300 mesh), which was activated for 2 h at 110 °C.[24–26] The column was equilibrated with 3–4 times column volume mobile phase (dichloromethane:methyl alcohol:H_2O = 8:2.5:0.5, V/V). The crude extract was dissolved in mobile phase and applied to the silica gel column (40 cm × 3.0 cm). The eluent was collected by fraction size of 5 mL and tentative identification was carried out using TLC. Gradually increasing the proportion of strongly polar in mobile phase and the finally elution at a constant flow rate of 1 mL/min. The eluent was collected by fraction size of 6 mL and the tentative identification was carried out using TLC. Collected the fractions of the same composition and concentrated through vacuum concentration. Get dry sample by vacuum pump equipment and measured the purity of sample by HPLC.

Crystallization process

The experiments of primary crystallization process were performed in a 250 mL crystallizer whose temperature was controlled by a water bath. According to the boiling point of solvent, 100 mL extract solution at 40 °C was prepared in the crystallizer and kept spin with rate of 60 rpm for evaporative crystallization. After filtration, the crystals obtained were dried in a vacuum oven at the temperature of 40 °C for 8 h. The recrystallization of primary crystallization was carried out in methanol with low temperature reactor whose system was cooled down to 10 °C at a constant rate of 1.0 °C/min. Followed by filtration and drying.[27,28]

DSC and TGA analysis

The thermal properties of sample were analyzed by performing differential scanning calorimeter (DSC). Assay preparation: 3–5 g solid sample was weigh and pressed into piece in a little aluminum dish, an empty aluminum dish was used as the comparison. Determination conditions: testing temperature covers the range of 20–200 °C, heating rate: 10 °C/min, nitrogen as the carrier gas and flow rate 20 mL/ min.

The relationship between quality and temperature variation of the sample was measured by thermo gravimetric analyzer (TGAQ500, TA, USA). Determination conditions: Sample 3–5 mg, nitrogen environment (static), the testing temperature covers the range of 20–800 °C, heating rate: 10 °C/min.

Monosaccharide composition analysis

The monosaccharide compositions of the sample were determined by gas chromatography (Varian 4000 GC–MS).[29] 5.0 mg sample was hydrolyzed with 1 mL of 2 M trifluoroacetic acid (TFA) in a sealed scale test tube with N_2 protecting and heating at 110 °C for 3 h in an oil bath. Residual acid was removed by repeatedly co evaporation with anhydrous methanol. Hydrolyzed sample (2 mg) was mixed with hydroxylamine hydrochloride (10 mg) and internal standard inositol (2 mg). Then pyridine (0.5 mL) was added in and reacted at 90 °C for 30 min. After cooling down, acetylation reaction was conducted with the addition of acetic anhydride (0.5 mL) at 90 °C for 30 min. The final product was dried by rotary evaporation and dissolved in 1 mL methylene chloride. Ultimately, the solution was analyzed by GC–MS. d-glucose, d-galactose, l-rhamnose, d-xylose, d-mannose, and l-arabinose were also derivated as standards.

Specific rotatory power identification

The sample (10 mg) was dissolved in methyl alcohol (1 mg/mL). Zero the polarimeter with methyl alcohol. Optical rotation was analyzed with a WZZ-2B at 25 °C and calculated as follows:

$[\alpha]_t^{\lambda} = \frac{\alpha}{L \times C}$; α is the optical rotation; t is the temperature; λ is the wavelength of light source (589 nm); L is the length of polariscope tube; C is the CG-1 concentration (g/mL).

FT-IR, NMR and MS analysis

Mixtures of sample (1 mg) and dry KBr (150 mg) were pressed into a 1 mm thick disk for FT-IR spectrometer measurement from 4000 to 400 cm^{-1} (VECTOR-22). The sample was dissolved in 0.6 mL of CD_4O and kept completely dissolved. The ^{1}H NMR, ^{13}C NMR and HMQC spectra were recorded on a Bruker spectrometer at a probe temperature of 298 K and operated at 400 MHz.

Mass spectrometry conditions: Sample concentration was 10–50 ppm, mobile phase was chromatographic grade acetonitrile and methanol (1:1, V/V), the purified sample solution was directly collected by mass spectrometer section (IF-TOF) equipped with ESI sources.

Antioxidant activity tests in vitro

ABTS radical scavenging assay. ABTS radical reaction ($ABTS^{+}$) solution preparation: according to 1:1 mix ABTS (7 mM) and anthion solution (2.45 mM) and keep 12–16 h at room temperature in dark. Dilute with pH 7.4 phosphate buffer (0.1 mM) until the absorption value to 0.7 ± 0.02 at 734 nm. The diluted solution (2 mL) was mixed with 0.2 mL sample solution, and the mixture solution was incubated for 6 min at room temperature. The absorbance was measured at 734 nm. The scavenging activity on ABTS radical was calculated by the following formula:

$$SR1(\%) = \left[1 - \frac{Ai - Aj}{Ao}\right] \times 100\% \quad (1\text{-}1)$$

Ai: the absorbance of the ABTS radical solution with tested samples; Aj: the absorbance of ethanol solution with tested samples; Ao: the absorbance of the ABTS radical solution without sample.

DPPH radical scavenging assay

Free radical scavenging activity was determined using the conventional DPPH**.** method. Various test samples (2 mL) were added

to the solution of DPPH**.** (2mL, 0.2 mM). After a 30 min incubation period at 25 °C, the absorbance was determined against a blank at 517 nm. The free radical inhibition by DPPH**.** in percent (SR1%) was calculated as follows:

$$SR2(\%) = \left[1 - \frac{Ai - Aj}{Ao}\right] \times 100\% \quad (1\text{-}2)$$

Ai: the absorbance of 2 mL test samples solution and 2 mL DPPH**.** solutions; Aj: the absorbance of 2 mL test samples solution and 2 mL absolute ethanol solution; Ao: the absorbance of 2 mL DPPH solution and 2 mL anhydrous ethanol solution.

Superoxide radical scavenging activity assay

Pyrogallol autoxidation was used in this experiment; the specific steps were mentioned as follows: Place 50 mM, Tris-HCl buffer (pH 8.2) of 340 μL in the 1.5 mL centrifuge tube before it was bathed at 25 °C for 20 min. Then adding test samples 100 μL and 50 μL Benzene three phenol solutions (25 mM). The reaction continued 4 min at 25 °C, then terminating the reaction with 10 μL hydrochloric acid solution (8 mM). Result was carried out by measuring the absorbance value of at 300 μL reaction mixture, which was placed in a 96-well microtiter plates. The formula shown in Formula:

$$SR3(\%) = \left[1 - \frac{Ai - Aj}{Ao}\right] \times 100\% \quad (1\text{-}3)$$

Ai: absorbance of pyrogallol solution containing samples; Aj: absorbance of solution containing samples without pyrogallol; Ao: absorbance of pyrogallol solution containing distilled water as much as sample.

Hydroxyl radical scavenging assay

The specific steps of the experiment of capacity to scavenge **.**OH were mentioned as follows: Place 200 μL ferrous sulphate Solution (6 mM), 200 μL hydrogen dioxide solution (6 mM) and 100 μL test samples, then shaking up and placing at room temperature 20 min. Adding 200 μL salicylic acid solution (6 mM) and shaking up. The reaction continued 60 min at 37 °C, then placed stably for 10 min. Result was carried out by measuring the absorbance value of at 300 μL reaction mixture at 510 nm, which were placed in a 96-well microtiter plates. The formula shown in Formula:

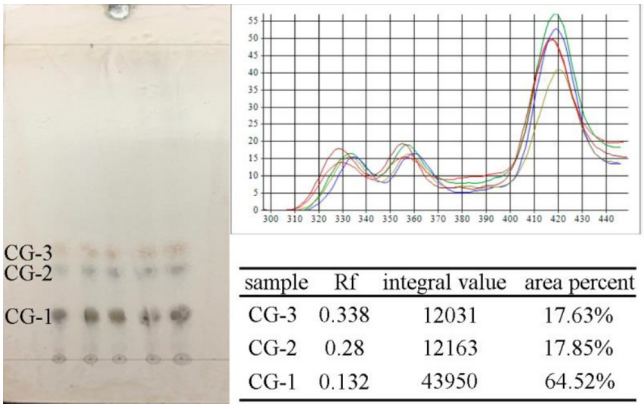
$$SR4(\%) = \left[1 - \frac{Ai - Aj}{Ao}\right] \times 100\% \quad (1\text{-}4)$$

Ai: absorbance of reaction solution containing samples; Aj: absorbance of samples solution; Ao: absorbance of reaction solution containing distilled water as much as sample.

Results and discussion

Separation by silica gel column chromatography

Experiments indicate that *Imperial Chrysanthemum* glucoside (CG) could be separated through the developing solvent (dichloromethane:methyl alcohol:H_2O = 8:2.5:0.5, V/V) effectively, and the Rf of CG-1, CG-2 and CG-3 were 0.132, 0.28 and 0.338. The percentages of relative content were 64.52%, 17.85% and 17.63% (Fig. 1**A**). CG-1 and the mixture of CG-2 and CG-3 were separated with the mobile phase which made up of dichloromethane, methyl alcohol and H_2O with the volume ratio of 8: 2.5: 0.5 (Fig. 1**B**). The yield of CG-1 was 3.7 mg/g. The yield of CG-2 & CG-3 was 1.8 mg/g. A unified and purified CG-1 was obtained as it could be observed in the HPLC (Fig. 1**C**). The weak peak appeared at 3.74 min and its neighboring negative peak was caused by the acetonitrile in



sample	Rf	integral value	area percent
CG-3	0.338	12031	17.63%
CG-2	0.28	12163	17.85%
CG-1	0.132	43950	64.52%

Fig. 1a. Thin-layer chromatography and imaging analysis.

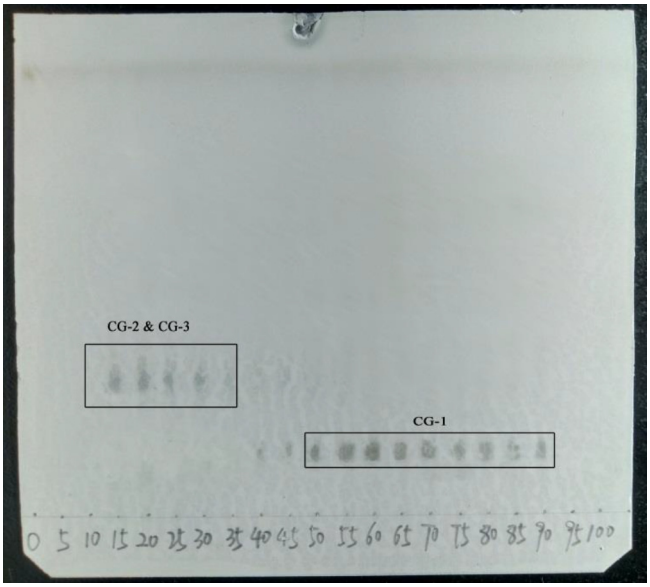


Fig. 1b. The TLC test of collecting liquid from column chromatography.

mobile phase (acetonitrile: H_2O = 3: 1). The strong peak at 4.40 min was the response of CG-1.

Crystallization, DSC and TGA analysis

Fig. 2 showed that the crystal shape of CG-1 under a microscope. According to the observations from different angles, concluded that the crystal shape is combination, which consist of a quadrangular and two rectangular pyramids.

Melting point is one of the physical data which was used to be measured by DSC.[30,31] This method was recommended by International Congress on Thermal Analysis and Calorimetry (ICTAC). The error between the accuracy of determination and thermodynamic equilibrium temperature can reach ± 1 °C. As is shown in Fig. 3, point B was the starting temperature, point D was the peak temperature, and point E was the final temperature. Point B was the intersection of the extended line of baseline and the tangent which have maximum slope at the leading edge of the peak. And the temperature of point B was named extrapolated onset temperature, which was the same as thermodynamic equilibrium temperature (melting temperature). The melting point of CG-1 crystal was 150.22 °C.

As it could be observed from TGA curves of CG-1 (Fig. 4), when the temperature reached 149.83 °C, the mass of CG-1 started to fall. There was no associated water existence in CG-1. It was at this

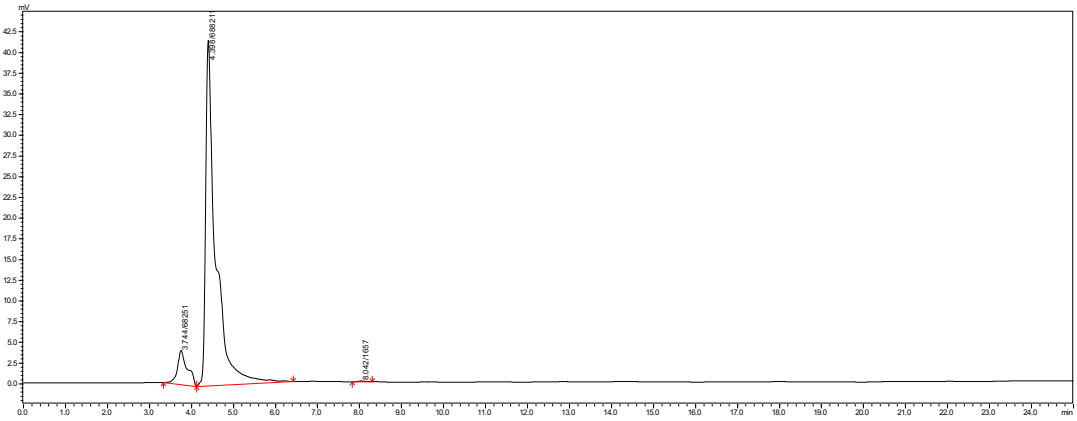


Fig. 1c. HPLC profile of CG-1.

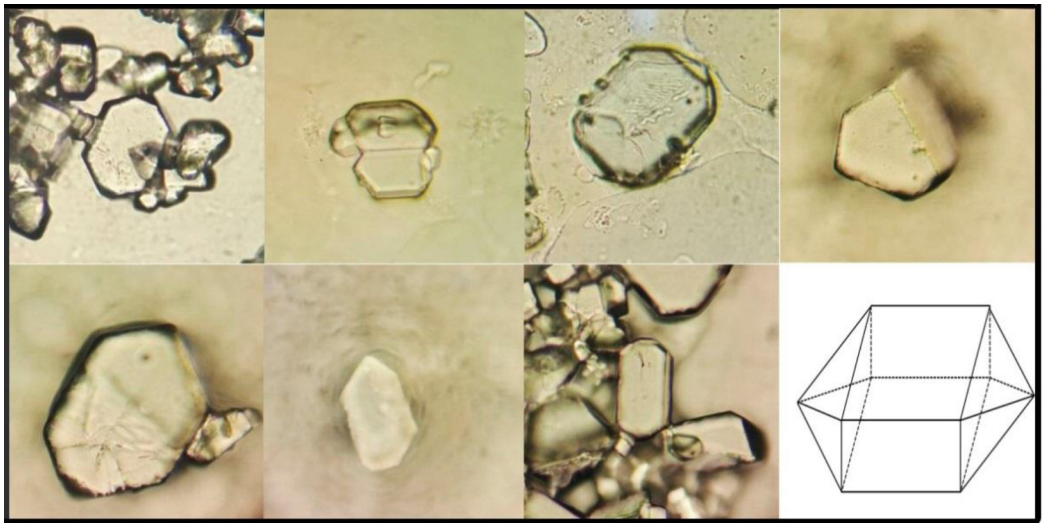


Fig. 2. The crystal of CG-1.

temperature that CG-1 has been finished transition from a solid to a liquid. Along with the rise of temperature, the rate of weight loss of CG-1 increased gradually. Until the temperature rose to 193.80 °C the weight of CG-1 began to decline significantly. It may be caused by evaporation of liquid CG-1. When the temperature reached 273.03 °C, the lower rate of sample was changed caused by pyrogenic decomposition and other chemical reaction. However, as the temperature reached 400 °C, the decrease of qualities become slower. Up to 800 °C, there was an 88.79% weight loss of CG-1.

Monosaccharides analysis

As it was shown in Fig. 5, standard monosaccharides were separated rapidly within 30 min. The peaks of standard monosaccharides were identified in the order of l-Rhamnose, d-Arabinose, d-Xylose, d-Mannose, d-Glucose, and d-Galactose. The samples were identified by matching their retention times with those of standard monosaccharides under the same analytical conditions. The results showed that CG-1 contains only d-Glucose.

FT-IR, NMR and MS, analysis

Infrared spectrum of CG-1 revealed the major functional groups and the chemical bonds (Fig. 6). The wide and strong band around 3389.28 cm^{-1} exhibited the presence of hydroxyl stretching vibration.[32] The bands at 1103.89 cm^{-1}, 1105.64 cm^{-1} and 1128.19 cm^{-1} belong to primary alcohol, secondary alcohol and tertiary alcohol respectively. The three characteristic absorption peaks around 1050 cm^{-1} was attributed to pyranring, which indicated the existence of pyranose in CG-1. The band in the region of 2941.60 cm^{-1} was due to C—H stretching vibration. And the weak bands near 1400 cm^{-1} belonged to C—H bending. The bands around to the region of 2514.25 cm^{-1} were due to mercaptan (—SH). There were no characteristic absorption peaks at the region of 1800 cm-1 to 1700 cm^{-1} means no aldehyde and carboxyl. So the band at 1632.63 cm^{-1} assigned to OH bending vibrations or H_2O or five-member ring. The absorption bands at 1070.22 cm^{-1}, corresponding characteristic of ethers, indicated the possible presence of ether linkage in CG-1. Absorptions at 845.18 cm^{-1} were typical for alpha-dominating configuration in pyranose.[33]

The 400-MHz ^1H, ^{13}C NMR and HMQC spectra of each fraction are shown in Fig. 7. The ^1H signal at 4.7906 ppm is due to H_2O. The chemical shifts from 3.5 to 4.5 ppm were assigned to the protons of carbons C-2′ to C-6′ of the glycosidic ring. The peak at 5.2823 ppm was attributed to the signal of anomeric proton which was the typical signals of glucoside. The result was in agreement with the analysis of monosaccharide composition. ^1H signals appeared in the anomeric region of 5.12–5.44 ppm, which indicated that the sample existed in the alpha-type configuration.[34]

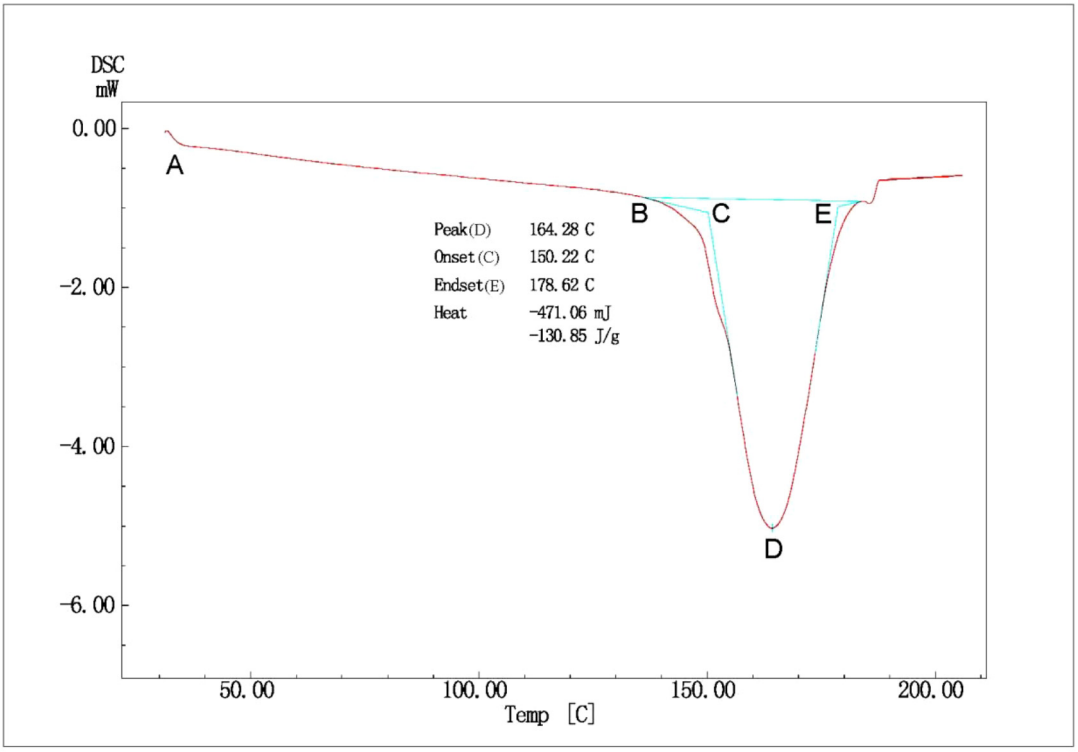


Fig. 3. DSC curves of CG-1.

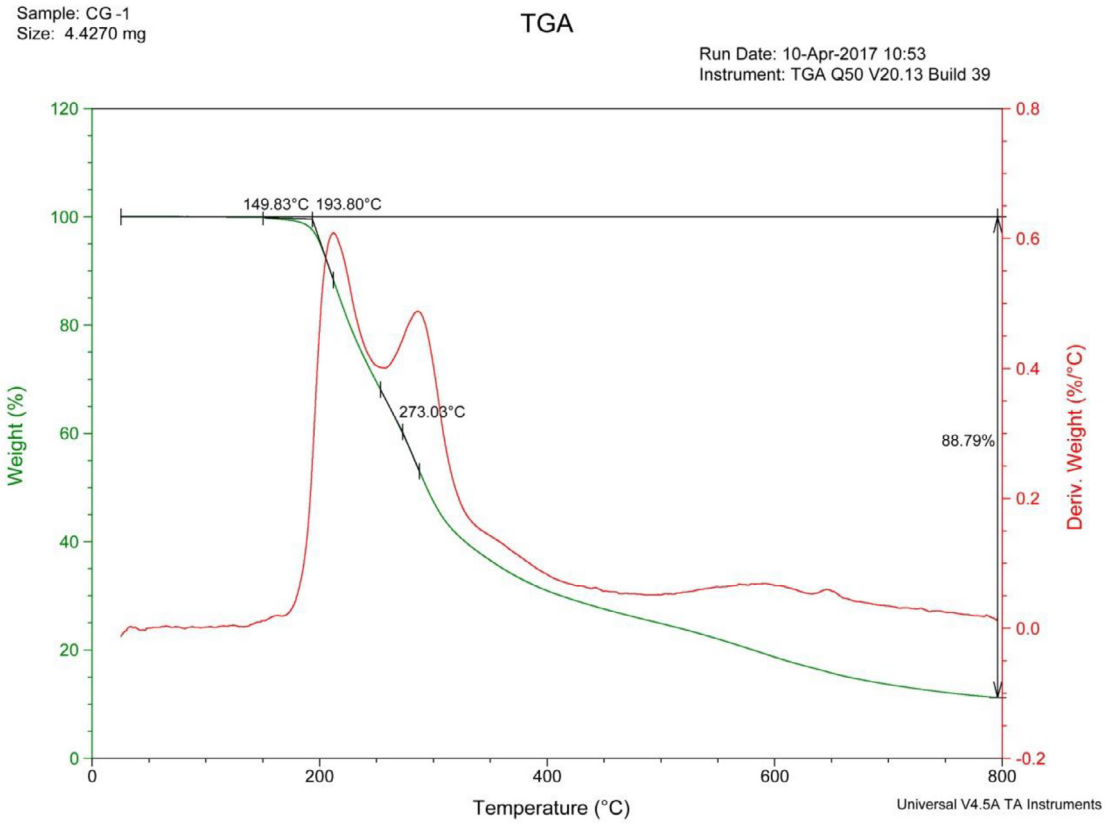


Fig. 4. TGA curves of CG-1.

The stereochemistry of the newly introduced linkage was determined to be alpha on the basis of the Glu H-1, H-2 coupling constant (J = 3.8 Hz). This result is consistent with the result of FT-IR.

The optical rotation of CG-1 was -39° at 25 °C. ^{1}H NMR (400 MHz, CD_4O, δ ppm): 5.29 (d, J = 3.8 Hz, 1H, H-1′), 3.73 (m, 1H, H-2′), 3.92 (t, J = 8.12 Hz, 1H, H-3′), 3.65 (s, 1H, H-4′), 3.26 (dd,

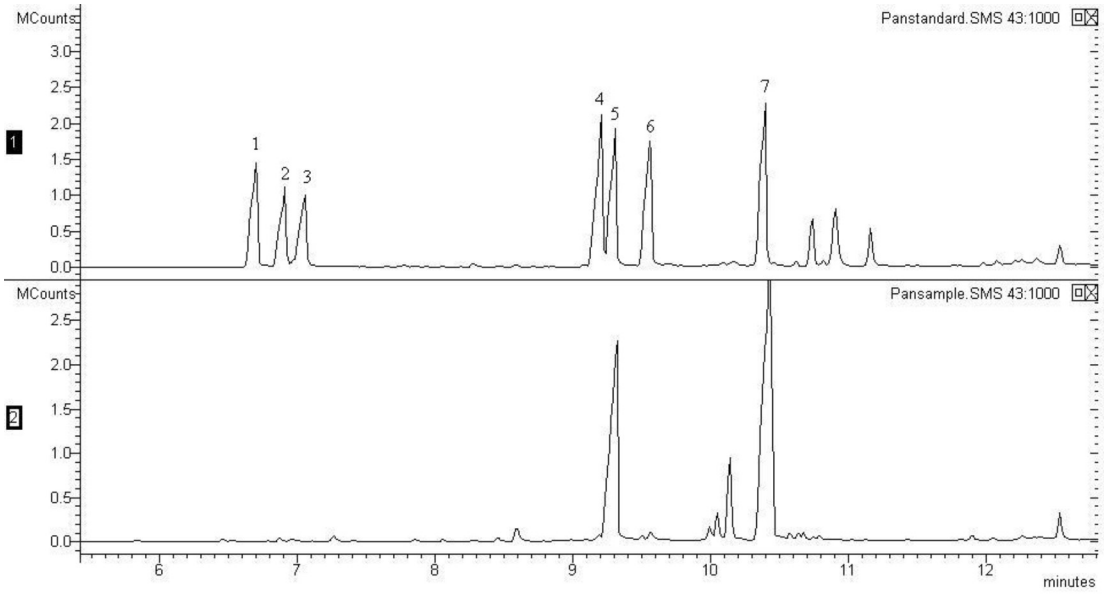


Fig. 5. The GC chromatograms of derivatives of 6 standard monosaccharides and CG-1.Peaks: (1) L-Rhamnose, (2) D-Arabinose, (3) D-Xylose, (4) D-Mannose, (5) D-Glucose, (6) D-Galactose, (7) interior label.

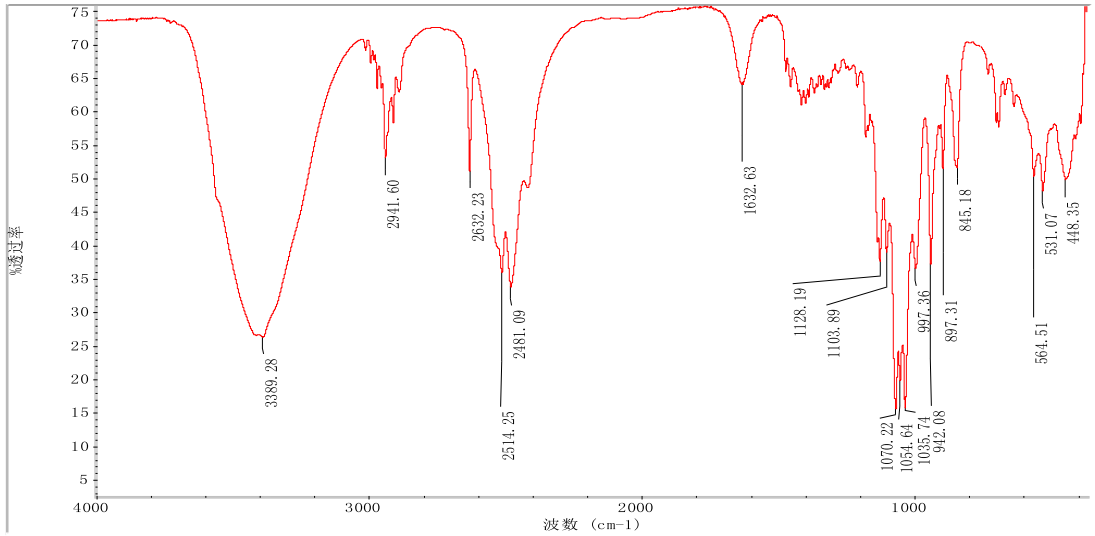


Fig. 6. FT-IR spectra of CG-1.

J_1=9.5 Hz, J_2=3.64 Hz,1H, H-5′), 3.62,3.69 (m,2H, H-6′), 3.59 (t, J = 4.62 Hz, 2H, H-1), 3.67 (d, J = 4.6 Hz, 1H, H-2), 3.52 (q, 2H, H-4), 4.00 (d, J = 8.2 Hz, 1H, H-5), 3.33 (dd, J_1 = 3.76 Hz, J_2=9.8 Hz,2H, H-6). MS (ESI) m/z: 365.0872, $[M+Na]^+$.

As shown in Fig. 8, the signal at 92.22 ppm was assigned to the anomeric carbons (C-1′) and indicated that the sample existed in the alpha-type.[33,34] The result was in agreement with the analysis of FT-IR and ^{1}H NMR. Other carbons atoms were bound to oxygen atoms according to the peak positions of ^{13}C NMR spectroscopy. Making an extrapolation according to the carbon spectrum, there was no carbon–carbon or carbon oxygen double bond, which consistent with the analysis of FT-IR. And the cause of the degrees of unsaturation was the existence of ring structure in molecular. ^{13}C NMR (400 MHz, CD_4O, δ ppm): 92.22 (C-1′), 73.00 (C-2′), 74.29 (C-3′), 61.95 (C-4′), 69.92 (C-5′), 60.79 (C-6′), 73.25 (C-1), 82.41 (C-2), 103.92 (C-3), 62.62 (C-4), 77.91 (C-5), 71.82 (C-6).

As is shown in Fig. 9, there is no hydrogen linked with the carbon, whose peak appeared at 103.92 in carbon spectrum, so the signal at 103.92 ppm was not the anomeric carbons.

ABTS assay is often used in evaluating total antioxidant power of compounds.[35] The ABTS radical scavenging activities were shown in Fig. 11**(a)**. The figure illustrated that the scavenging ability correlated well with increasing concentrations. CG-1 showed pronounced high radical scavenging activity, and the scavenging ability of the mixture of CG-2 & CG-3 was significantly lower than CG-1 and VC. Which were 33.11%, 83.33% and 96.78% respectively at the concentration of 2.5 mg/mL. Fig. 11**(b)** shows that the activity of CG-1 on inhibition of the DPPH radical was related to the concentration of the samples. In the scavenging ability of these different fractions tested, CG-1 was far greater than CG-2 & CG-3, which were 83.92% and 19.25% respectively at the concentration of 2.5 mg/mL. But, there is still a gap compared with VC.

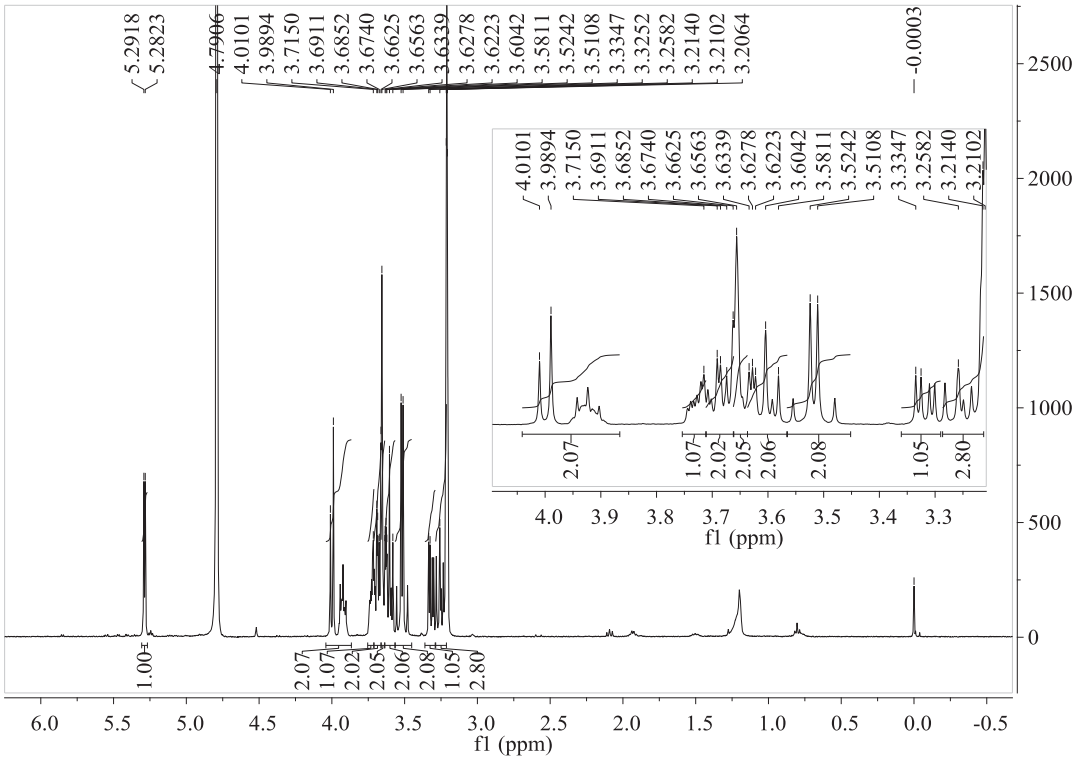


Fig. 7. The ^{1}H NMR spectrum of CG-1.

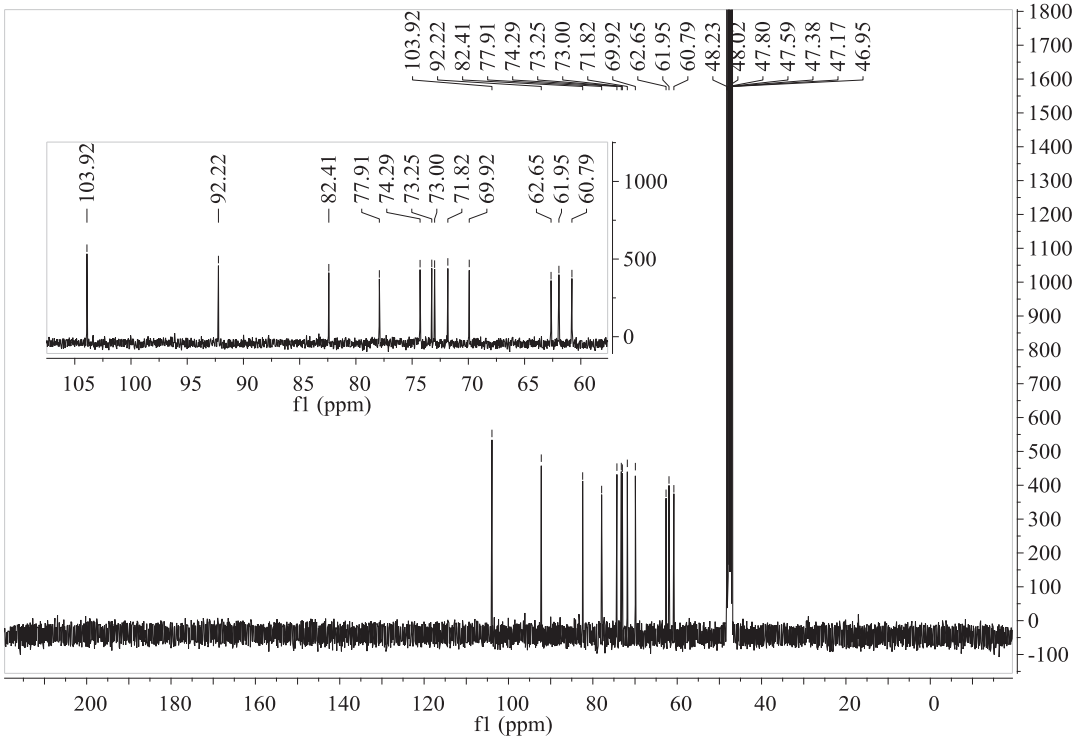


Fig. 8. The ^{13}C NMR spectrum of CG-1.

Superoxide radical is a highly toxic species that is generated by metabolic process and physical irradiation, and it is considered as the primary ROS.[36,37] The superoxide radical scavenging activities of the three fractions are shown in Fig. 11**(c)**. The scavenging activity of CG-1 correlated with increasing concentration. At concentration of 2.5 mg/mL, the scavenging rate of CG-1 and CG-2 & CG-3 were 73.92% and 19.25%, respectively. The superoxide radicals scavenging activity of VC was higher.

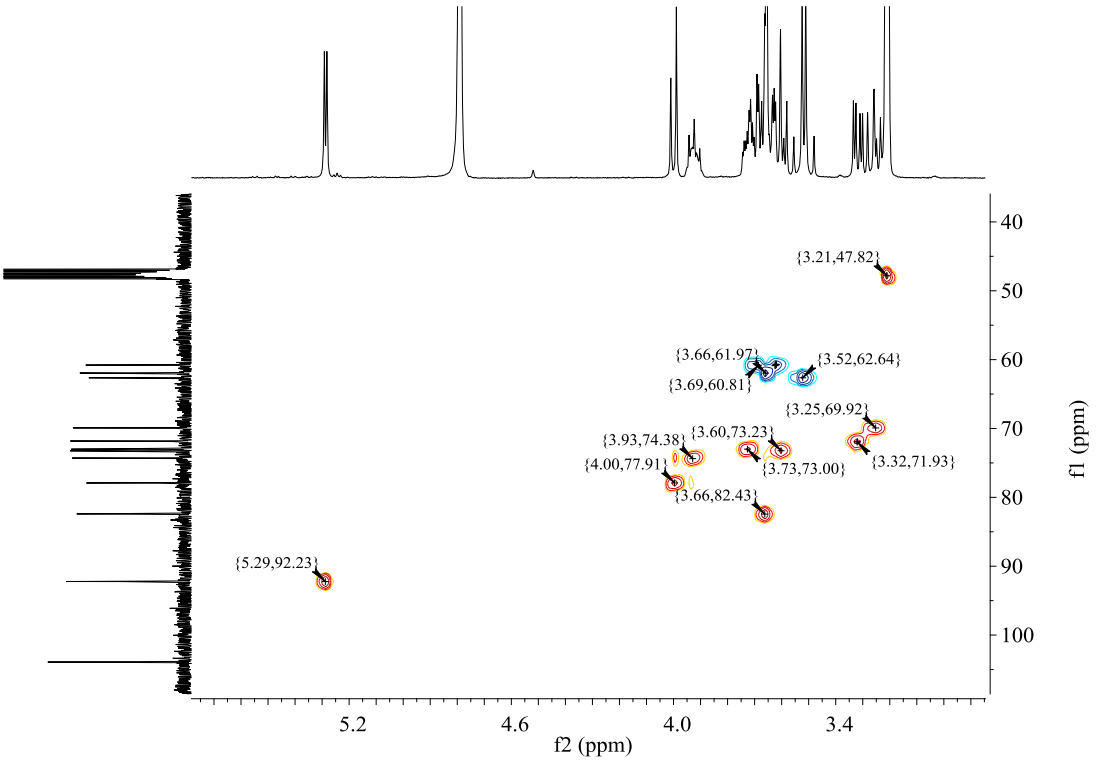


Fig. 9. The HMQC spectrum of CG-1.

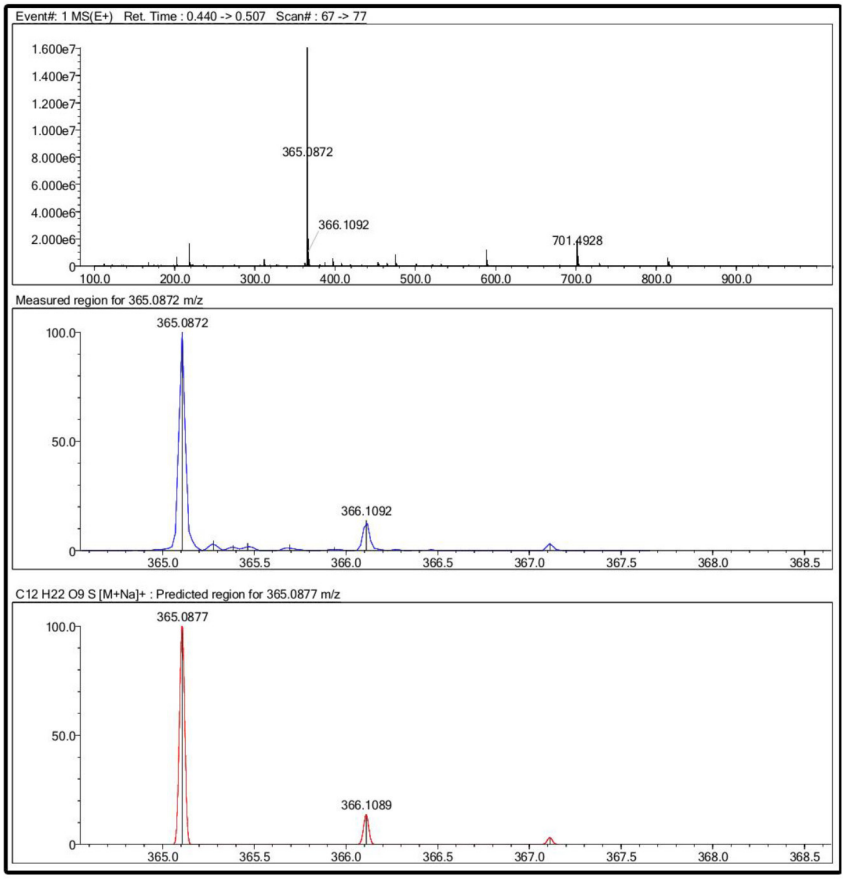


Fig. 10. Determination of Molecular Weight by HPLC-MS of CG-1.

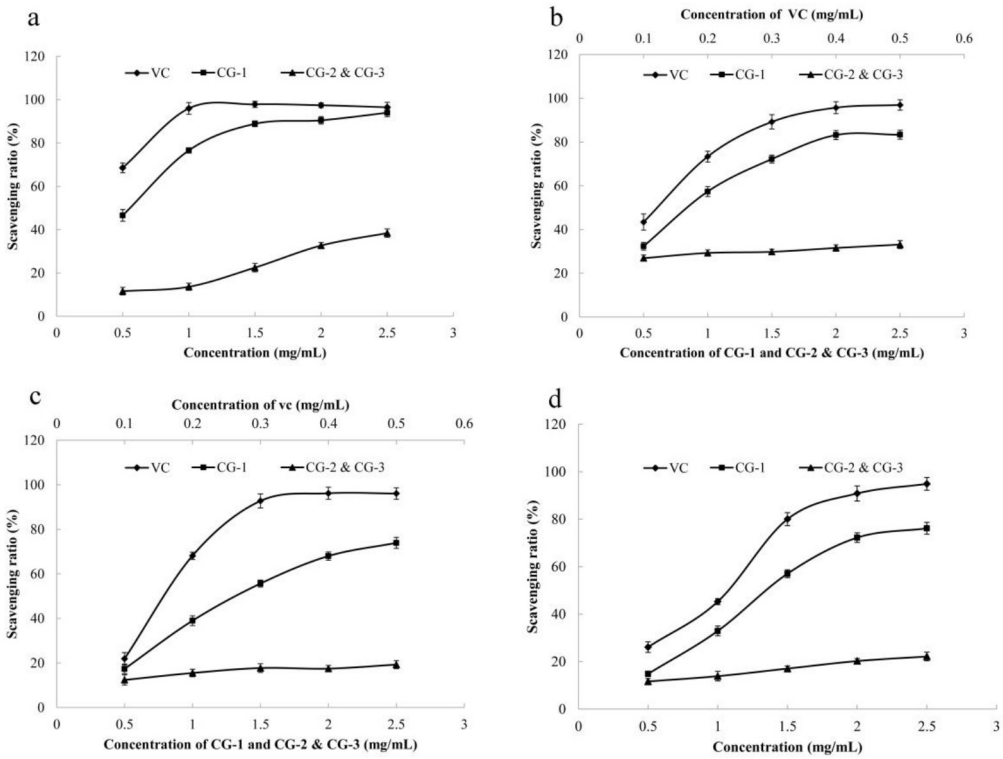


Fig. 11. Antioxidant activities of VC, CG-1 and CG-2 & CG-3: (a) ABTS radical scavenging activity, (b) DPPH radical scavenging activity, (c) superoxide radicals scavenging activity, (d) hydroxyl radical scavenging activity. VC was used as the positive control. Data are presented as means ± SD, n = 3.

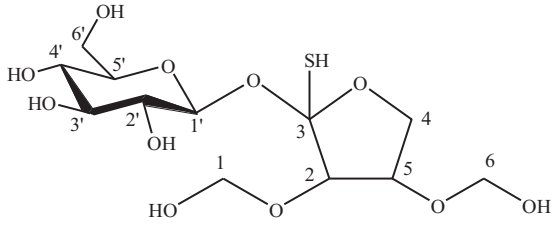


Fig. 12. The molecular structure of CG-1.

In this experiment, hydroxyl radical is generated from well-known Fenton reaction ($Fe_2^+ + H_2O_2 \rightarrow Fe_3^+ + {\cdot}OH + OH$), salicylic acid captures hydroxyl radical to form 2,3-dihydroxyl benzoic acid, and it had maximum absorbance at 510 nm. Fig. 11(d) described that, at 2.5 mg/mL, the hydroxyl scavenging abilities of VC, CG-1 and CG-2 & CG-3 were 94.89%, 76.15% and 22.14%, respectively. CG-1 showed obvious hydroxyl radical scavenging activity in a dose-dependent pattern. The hydroxyl radical scavenging ability was attributed to various mechanisms, such as suppression against hydroxyl radical generation, decomposition of peroxides and prevention of continued hydrogen abstraction. The possibility of scavenging hydroxyl radical by CG-1 was that it could supply of hydrogen and combine with radical to terminate the radical chain reaction, which consistent with the results of structural analysis.[38]

There is a slight gap in scavenging activity of ABTS radical and hydroxyl radical between CG-1 and VC. The scavenging activity of DPPH radical and superoxide radicals was certain disparity. But the scavenging activity of CG-1 was steadily improving with the increase of concentration. In balance, CG-1 has the ability to resist oxidation.

Conclusions

In conclusion, a kind of glucoside, designated as CG-1, was isolated from the *Imperial Chrysanthemum*. Melting point was 150.22 °C and displayed good thermal stability. In CG-1, glucoside was determined by GC–MS. And the FT-IR and NMR indicated that the glucoside was alpha-glucoside. ^{13}C NMR showed that CG-1 contained 12 carbon atoms and no double bond. According to above-mentioned analytical result and LC-MS analysis judged that molecular weight was 342.098 and the molecular formula was $C_{12}H_{22}O_9S$ (Fig. 10). Unsaturation, caused by cyclization rather than double bonds, was two. According to spectroscopic data infer to the molecular structure of CG-1, as shown in Fig. 12. The structure completely coincided with the data obtained by FT-IR, NMR and mass spectrometry. Compared to VC, the structure of CG-1 had similar parts. They are polyhydroxy compound and have similar five element ring, which contain oxygen. It may be the cause why CG-1 showed good antioxidant capacity.

Conflict of interest

We declare that we have no financial and personal relationships with other people or organizations that can inappropriately influence our work, there is no professional or other personal interest of any nature or kind in any product, service or company that could be construed as influencing the position presented in, or the review of, the manuscript entitled, "Structural analysis and antioxidant activity of the glycoside from *Imperial Chrysanthemum*"

Acknowledgments

This work was financially supported by the National Key Project of Research and Development Plan of China (2016YFD0400803)

and the key program of the Natural Science Foundation of Tianjin (16JCZDJC34100).

References

1. Seifried HE, Anderson DE, Fisher EI, Milner JA. A review of the interaction among dietary antioxidants and reactive oxygen species. *J Nutrit Biochem*. 2007;18(9):567–579.
2. Salvatore De Rosa PC, Antonella Paglia, Laura Sasso, Vito Di Palma M, assimo Chiariello. Reactive oxygen species and antioxidants in the pathophysiology of cardiovascular disease: does the actual knowledge justify a clinical approach? *Curr Vasc Pharmacol*. 2010;8:259–275.
3. Prasad S, Gupta SC, Tyagi AK. Reactive oxygen species (ROS) and cancer: Role of antioxidative nutraceuticals. *Cancer Lett*. 2017;387:95–105.
4. EWAN CAMERONt LP.. Supplemental ascorbate in the supportive treatment of cancer: revaluation of prolongation of survival times in terminal human cancer. *Med Sci*. 1978;75(9):4538–4542.
5. Zuo L, Otenbaker NP, Rose BA, Salisbury KS. Molecular mechanisms of reactive oxygen species-related pulmonary inflammation and asthma. *Mol Immunol*. 2013;56:57–63.
6. Meng D, Zhang P, Zhang L, et al. Detection of cellular redox reactions and antioxidant activity assays. *J Funct Foods*. 2017;37:467–479.
7. Blaszczyk A, Skolimowski J, Materac A. Genotoxic and antioxidant activities of ethoxyquin salts evaluated by the comet assay. *Chem Biol Interact*. 2006;162:268–273.
8. Blaszczyk A, Skolimowski J. Comparative analysis of cytotoxic, genotoxic and antioxidant effects of 2,2,4,7-tetramethyl-1,2,3,4-tetrahydroquinoline and ethoxyquin on human lymphocytes. *Chem Biol Interact*. 2006;162:70–80.
9. Shang X, Zhu Z-Y, Wang F, Liu J-C, Liu J-Y, Xie M-L. Hypoglycemic effect of Chrysanthemum morifolium extract on alloxan-induced diabetic mice is associated with peroxisome proliferator-activated receptor α/γ-mediated hepatic glycogen synthesis. *J Appl Biomed*. 2017;15:81–86.
10. Wen L, Zhao Y, Jiang Y, et al. Identification of a flavonoid C-glycoside as potent antioxidant. *Free Radical Biol Med*. 2017;110:92–101.
11. Nile SH, Nile AS, Keum YS, Sharma K. Utilization of quercetin and quercetin glycosides from onion (Allium cepa L.) solid waste as an antioxidant, urease and xanthine oxidase inhibitors. *Food Chem*. 2017;235:119–126.
12. Niu X, Xu D, Luo J, Kong L. Main iridoid glycosides and HPLC/DAD-Q-TOF-MS/MS profile of glycosides from the antioxidant extract of Eucommia ulmoides Oliver seeds. *Ind Crops Prod*. 2016;79:160–169.
13. Bai J, Fang ZF, Chen H, et al. Antioxidant phenolic glycosides from the roots of Illicium dunnianum. *Carbohydr Res*. 2012;361:206–211.
14. Pukalskas A, Venskutonis PR, Dijkgraaf I, van Beek TA. Isolation, identification and activity of natural antioxidants from costmary (Chrysanthemum balsamita) cultivated in Lithuania. *Food Chem*. 2010;122:804–811.
15. Fernandes L, Casal S, Pereira JA, Saraiva JA, Ramalhosa E. Edible flowers: a review of the nutritional, antioxidant, antimicrobial properties and effects on human health. *J Food Compos Anal*. 2017;60:38–50.
16. Chen LX, Hu DJ, Lam SC, et al. Comparison of antioxidant activities of different parts from snow chrysanthemum (Coreopsis tinctoria Nutt.) and identification of their natural antioxidants using high performance liquid chromatography coupled with diode array detection and mass spectrometry and 2,2′-azinobis (3-ethylbenzthiazoline-sulfonic acid)diammonium salt-based assay. *J Chromatogr A*. 2016;1428:134–142.
17. Periche A, Castello ML, Heredia A, Escriche I. Influence of drying method on steviol glycosides and antioxidants in Stevia rebaudiana leaves. *Food Chem*. 2015;172:1–6.
18. Wang S, Hao LJ, Zhu JJ, et al. Study on the effects of sulfur fumigation on chemical constituents and antioxidant activity of Chrysanthemum morifolium cv. Hang-ju. *J Phytother Phytopharmacol*. 2015;21(5):773–779.
19. Yuan J, Hao L-J, Wu G, et al. Effects of drying methods on the phytochemicals contents and antioxidant properties of chrysanthemum flower heads harvested at two developmental stages. *J Funct Foods*. 2015;19:786–795.
20. Zheng L, Van Labeke MC. Chrysanthemum morphology, photosynthetic efficiency and antioxidant capacity are differentially modified by light quality. *J Plant Physiol*. 2017;213:66–74.
21. El-Ghobashy MR, Fayez YM, Goda ZM, Shehata MA. HPLC and TLC chromatographic methods for simultaneous determination of binary mixture of isoconazole nitrate and diflucortolone valerate. *Bull Facul Pharm, Cairo Univ*. 2016;54:33–37.
22. Schulze C, Strehle A, Merdivan S, Mundt S. Carbohydrates in microalgae: comparative determination by TLC, LC-MS without derivatization, and the photometric thymol-sulfuric acid method. *Algal Res*. 2017;25:372–380.
23. Rokka J, Gronroos TJ, Viljanen T, Solin O, Haaparanta-Solin M. HPLC and TLC methods for analysis of [18F]FDG and its metabolites from biological samples. *J Chromatogr, B: Anal Technol Biomed Life Sci*. 2017;1048:140–149.
24. X-m Zhao, R-j Li, Zhou C, et al. Separation and purification of deoxynivalenol (DON) mycotoxin from wheat culture using a simple two-step silica gel column chromatography. *J Integrat Agri*. 2016;15:694–701.
25. Song W, Zhou Y, Fu Y, Xu W. Self-disproportionation of enantiomers of prazoles via achiral, gravity-driven silica gel column chromatography. *Tetrahedron Asymmetry*. 2013;24:909–912.
26. Tang D, Zhang L, Chen H, et al. Extraction and purification of solanesol from tobacco(I). Extraction and silica gel column chromatography separation of solanesol. *Sep Purif Technol*. 2007;56:291–295.
27. Yin Y, Yang Y, de Lourdes Mendoza M, et al. Progressive freezing and suspension crystallization methods for tetrahydrofuran recovery from Grignard reagent wastewater. *J Cleaner Prod*. 2017;144:180–186.
28. Wu D, Song L, Zhu C, Zhang X, Guo H, Yang C. Solubility of taurine and its application for the crystallization process improvement. *J Mol Liq*. 2017;241:326–333.
29. Ren YY, Zhu ZY, Sun HQ, Chen LJ. Structural characterization and inhibition on alpha-glucosidase activity of acidic polysaccharide from Annona squamosa. *Carbohydr Polym*. 2017;174:1–12.
30. Jin X, Xu X, Zhang X, Yin Y. Determination of the PCM melting temperature range using DSC. *Thermochim Acta*. 2014;595:17–21.
31. Charsley EL, Laye PG, Palakollu V, Rooney JJ, Joseph B. DSC studies on organic melting point temperature standards. *Thermochim Acta*. 2006;446(1–2):29–32.
32. Liu F, Zhu ZY, Sun X, Gao H, Zhang YM. The preparation of three selenium-containing Cordyceps militaris polysaccharides: Characterization and anti-tumor activities. *Int J Biol Macromol*. 2017;99:196–204.
33. Zhu ZY, Liu F, Gao H, Sun H, Meng M, Zhang YM. Synthesis, characterization and antioxidant activity of selenium polysaccharide from Cordyceps militaris. *Int J Biol Macromol*. 2016;93(Pt A):1090–1099.
34. Wang XT, Zhu ZY, Zhao L, et al. Structural characterization and inhibition on alpha-d-glucosidase activity of non-starch polysaccharides from Fagopyrum tartaricum. *Carbohydr Polym*. 2016;153:679–685.
35. Re R, Pellegrini N, Proteggente A, Pannala A, Yang M, Rice-Evans C. Antioxidant activity applying an improved abts radical cation decolorization assay. *Free Radical Biol Med*. 1999;26:1231–1237.
36. Liu J, Luo J, Ye H, Zeng X. Preparation, antioxidant and antitumor activities in vitro of different derivatives of levan from endophytic bacterium Paenibacillus polymyxa EJS-3. *Food Chem Toxicol*. 2012;50:767–772.
37. Song H, Zhang Q, Zhang Z, Wang J. In vitro antioxidant activity of polysaccharides extracted from Bryopsis plumosa. *Carbohydr Polym*. 2010;80:1057–1061.
38. He R, Ye J, Zhao Y, Su W. Partial characterization, antioxidant and antitumor activities of polysaccharides from Philomycusbilineatus. *Int J Biol Macromol*. 2014;65:573–580.